Catalysis
Science &
Technology

PAPER

View Article Online
View Journal

Check for updates

Cite this: DOI: 10.1039/c7cy02008b

Efficient Pt–FeO_x/TiO_2@SBA-15 catalysts for selective hydrogenation of cinnamaldehyde to cinnamyl alcohol

Yujie Xue, Ruihua Yao, Junrui Li, Guimei Wang, Peng Wu and Xiaohong Li*

TiO_2 was coated onto mesoporous silica SBA-15 by hydrolysis of tetrabutyl titanate to prepare 15 wt% TiO_2@SBA-15 composites (15TS). The 15TS composites retain the mesostructure of the SBA-15 host, and TiO_2 was highly dispersed and uniformly coated. 5 wt% Pt nanoparticles supported on 15TS were employed for liquid-phase selective hydrogenation of cinnamaldehyde (CAL) to cinnamyl alcohol (COL). Compared with the Pt catalyst supported on pristine SBA-15, the Pt/15TS catalyst afforded higher activity and selectivity to COL. Furthermore, the modification of the Pt/15TS catalyst by FeO_x can greatly improve the activity and selectivity to COL. As a result, the Pt–FeO_x/15TS catalyst displayed excellent selectivity to COL (around 84.5%) at nearly complete CAL conversion. Of particular note is that further calcination of the Pt–FeO_x/15TS catalyst precursor in air at 773 K before reduction would greatly enhance the catalytic performance. Consequently, the TOF reached 3.06 s^{-1} with a selectivity to COL of 86.4% over the Pt–FeO_x/15TS-773 catalyst. Moreover, the Pt–FeO_x/15TS-773 catalyst can also be reused about eight times without distinct loss in activity or selectivity. Based on characterization by XPS and H_2-TPR, the important promotion effect of FeO_x and strong metal–support interaction played key roles in preferential adsorption and activation of C=O bonds in CAL.

Received 30th September 2017,
Accepted 13th November 2017

DOI: 10.1039/c7cy02008b

rsc.li/catalysis

1. Introduction

Chemoselective hydrogenation of α,β-unsaturated aldehydes at carbonyl (C=O) groups to produce α,β-unsaturated alcohols is an important reaction. As a particularly important representative of α,β-unsaturated aldehydes, selective hydrogenation of cinnamaldehyde (CAL) can produce cinnamyl alcohol (COL), which is generally considered as one of the most challenging and valuable intermediates and then largely used in several chemical industries such as perfumes, flavors, and pharmaceuticals.[1–6] However, owing to the fact that C=O bonds bear a higher bond energy than C=C bonds (715 kJ mol^{-1} *versus* 615 kJ mol^{-1}, respectively),[7] the hydrogenation of C=C bonds is more thermodynamically favorable.[8] Therefore, the development of catalysts for the selective hydrogenation of CAL to COL remains a difficult challenge.[9] As is well known, chemoselectivity is affected by considerable parameters, so that the rational design of active and selective catalysts for selective hydrogenation of CAL is not an easy task. Thus, people have made many efforts in selective hydrogenation of CAL to COL during the past decades.[10–14]

Noble metal-based catalysts have been widely used for the hydrogenation of CAL.[8,15–21] Pd and Rh generally displayed high activities but rather poor selectivities towards COL.[22] Comparatively, Pt and Ru are commonly used metals exhibiting relatively higher catalytic performance to obtain the desired unsaturated alcohol.[14,19–21,23] In addition, the promotion of Pt catalysts by transition metals like Fe, Co, Sn, Zn or Cu can greatly improve the selectivity toward the unsaturated alcohol.[24–29] For instance, SiO_2-supported Pt–Fe catalysts were prepared to study their structure, chemisorptive, and catalytic properties promoting the selective hydrogenation of C=O bonds and the formation of α,β-unsaturated alcohols.[25] In addition, Pt–Zn and Pt–Fe catalysts supported on mesoporous carbon materials were applied for CAL hydrogenation, both of which improved the activity and induced a remarkable increase in selectivity to COL.[28] There are other examples, such as Pt–Fe/CNTs (carbon nanotubes) and Pt–Co/CNTs which displayed high activity and selectivity to COL as well.[27] Besides, a SnO_2-isolated Pt_3Sn alloy on reduced graphene oxide served as an efficient catalyst for selective hydrogenation of C=O in unsaturated aldehydes and furnished up to 92.5% selectivity to COL at a CAL conversion of 93.9% under mild conditions.[29]

Moreover, the electronic and stereo-hindrance effects would affect the adsorption mode of CAL on the catalyst surface; however, the key factors that control the activity and

---

Shanghai Key Laboratory of Green Chemistry and Chemical Processes, School of Chemistry and Molecular Engineering, East China Normal University, 3663 North Zhongshan Rd., Shanghai 200062, China. E-mail: xhli@chem.ecnu.edu.cn; Fax: +86 21 62238590; Tel: +86 21 62238590

selectivity in the hydrogenation of CAL are still unclear.[24,30] Because the interaction between the support and metal can modulate the surface electronic properties of the active metal, it would be a feasible way to adopt appropriate materials to load Pt nanoparticles for the liquid-phase hydrogenation of CAL. Since Tauster and Fung found that a strong metal–support interaction existed between noble metals and TiO_2 in the late 1970s,[31] application of reducible supports such as TiO_2 (ref. 32–34) and CeO_2 (ref. 35) aroused intensive interest. For instance, Pt/TiO_2 and Ni/TiO_2 catalysts were investigated in the hydrogenation of aldehydes.[33,36] In addition, 2 wt% Ru/TiO_2 and 4.7 wt% Sn/TiO_2 catalysts were also studied for the hydrogenation of methyl oleate.[37] It was proved that the strong interaction between metal and TiO_2 suppressed the migration and aggregation of metal particles on the TiO_2 surface.[30,33,36–39] Thus, the strong interaction would influence the surface electronic properties of noble metals and likely in turn bring considerable changes in their activity in catalytic reactions. Nevertheless, TiO_2 has serious disadvantages when used as a catalyst support itself. First, TiO_2 usually has small specific surface area, so that the adsorption and concentration of reactants around the active centers are limited.[40] Second, the required liquid–solid separation is difficult due to the formation of milky dispersion once the TiO_2 powder catalyst is mixed in water.[41] Therefore, we attempt to introduce TiO_2 onto the SBA-15 surface to prepare TiO_2@SBA-15 composites.

It is well known that SBA-15 has high specific surface area, large pore volume and adjustable pore size, which make it an ideal support for the preparation of highly dispersed heterogeneous catalysts.[39,42,43] The introduction of TiO_2 onto the SBA-15 surface can produce TiO_2@SBA-15 composites, which not only take advantage of mesoporous materials with large specific surface area and pore volume, but also exhibit properties not found in bulk TiO_2 alone. In our previous studies, it has been proved that TiO_2@SBA-15 composite-supported Pt catalysts behaved much better than TiO_2 or SBA-15 supported ones for liquid-phase hydrogenation of benzaldehyde.[44] It is anticipated that the TiO_2@SBA-15 composite-supported Pt catalysts can still show striking catalytic performance in the liquid-phase selective hydrogenation of CAL (Scheme 1). To further enhance the catalytic behaviors, FeO_x with an optimal amount was also doped to the Pt/TiO_2@SBA-15 catalyst for the tested reaction. To our delight, the FeO_x-doped Pt/TiO_2@SBA-15 catalyst afforded high activity and selectivity to COL and could be easily recycled several times without obvious loss in activity or selectivity to COL.

2. Experimental

2.1. Catalyst preparation

SBA-15 was synthesized according to the literature.[45] 15 wt% TiO_2@SBA-15 (15TS) composites were prepared by hydrolysis of tetrabutyl titanate (TBT) onto SBA-15 *via* a sol–gel method.[44] A typical procedure for the preparation of 15TS was as follows: SBA-15 was sonicated in isopropanol for 2 h (the mass ratio of SBA-15 to isopropanol is 1 : 15) and then, the required amount of TBT was added dropwise with stirring for 1 h. Then, water was slowly added and the stirring was maintained for an extra 2 h to complete the hydrolysis of TBT. The as-prepared materials were recovered by filtration, rinsed with deionized water and ethanol, dried at 353 K overnight, and finally calcined at 623 K for 2 h.

The 5 wt% Pt/15TS catalyst was prepared *via* an impregnation method using an ethanolic solution of H_2PtCl_6. The suspension was stirred for 4–6 h at room temperature, then evaporated to remove the excess solvent, followed by drying overnight at 353 K, and finally reduced in an aqueous solution of sodium formate at 363 K for 2 h. For comparison, 5 wt% Pt/TiO_2 and 5 wt% Pt/SBA-15 catalysts were also prepared using the same method.

The Pt–FeO_x/15TS catalyst containing 5 wt% Pt and 0.36 wt% Fe (where the Fe/Pt molar ratio is 0.25) was prepared using the similar method to that for the Pt/15TS catalyst, except that the ethanolic solution of H_2PtCl_6 and $FeCl_3$ were added together to impregnate 15TS composites. Additionally, some catalyst precursors before reduction were also calcined in air at 473 K or 773 K for 2 h and the resultant catalysts were denoted as Pt–FeO_x/15TS-*T*, where *T* represents the calcination temperature in Kelvin for the catalyst precursor.

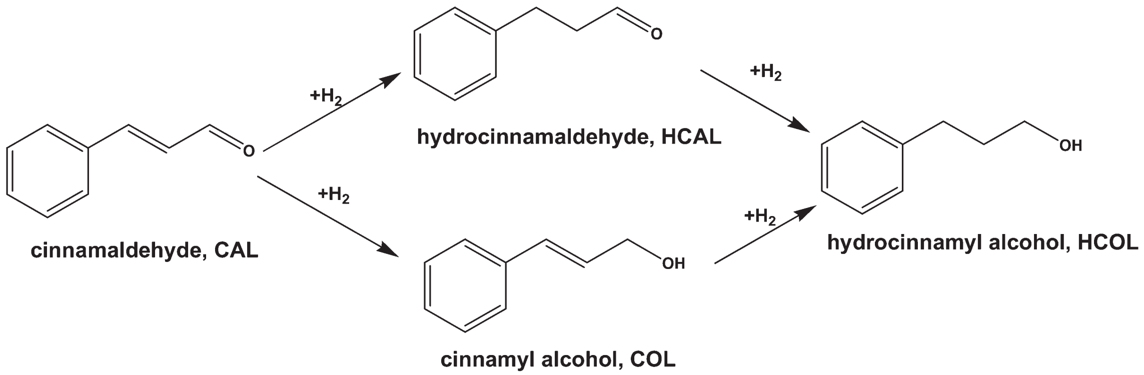

Scheme 1 Selective hydrogenation of CAL.

2.2. Characterization

Powder X-ray diffraction (XRD) patterns of the samples were collected on a Bruker D8 ADVANCE instrument using Cu Kα radiation (λ = 1.54178 Å) as the X-ray source. The N_2-physisorption isotherms of the samples were measured at 77 K on a Quantachrome Autosorb-3B system after the samples were evacuated at 573 K for 4 h. The Brunauer–Emmett–Teller (BET) specific surface area was calculated using adsorption data in the relative pressure range from 0.05 to 0.35. The pore size distribution curves were calculated from analysis of the adsorption branch of the isotherm using the Barrett–Joyner–Halenda (BJH) algorithm. The morphology of the samples was measured by scanning electron microscopy (SEM) using a Hitachi S4800 electron microscope with an accelerating voltage of 20 kV. The transmission electron microscopy (TEM) images were taken on an FEI Tecnai G2-TF30 microscope at an accelerating voltage of 300 kV. The amount of Pt atoms leached into the filtrate after recycling reaction was determined by inductively coupled plasma-atomic emission spectroscopy (ICP-AES) using a Thermo Elemental IRIS Intrepid II XSP.

The surface electronic properties of Pt were examined using X-ray photoelectron spectroscopy (XPS) with a Thermo Fisher Scientific ESCALAB 250Xi spectrometer with Al Kα radiation (1486.6 eV) as the incident beam with a monochromator. The samples were pre-treated *in situ* in flowing hydrogen at 673 K for 2 h in a reactor attachment of the XPS spectrometer. For comparison, the as-calcined samples without reduction were also probed by XPS. The binding energy (BE) was calibrated using C–C binding energy at 284.4 eV in order to compare the BEs with the data from the literature. The spectra shown in the figures have been corrected by Shirley background subtraction. Spectral fitting and peak integration was performed using XPSPEAK software. During deconvolution of XPS spectra, the FWHM (full width at half maxima) were set at 1.8 and 2.5 eV for Pt^0 and Pt^{2+} species, respectively. The Lorentzian–Gaussian ratio was set to 20%.

Temperature-programmed reduction with hydrogen (H_2-TPR) was conducted to investigate the interaction between Pt and the support or FeO_x with a Micromeritics AutoChem II chemisorption analyzer. Prior to H_2-TPR experiments, 250 mg of the catalyst was pre-treated at 573 K in flowing Ar for 1 h and then cooled to room temperature in flowing Ar (99.999%, 50 mL min^{-1}). After that, the sample was heated from room temperature to 1193 K with a heating rate of 10 K min^{-1} under a mixture of 10% H_2–Ar (50 mL min^{-1}). The rate of H_2 consumption was monitored by a gas chromatograph (GC) with a thermal conductivity detector (TCD).

2.3. Catalytic test

A certain amount of the catalyst was pre-treated in a specially-designed quartz tube under a hydrogen atmosphere (99.999% purity, 30 mL min^{-1}) at 673 K for 2 h before use. The catalyst was then immediately mixed with solvent (containing isopropanol and water in a volume ratio of 9 : 1) and CAL without further exposure to air, which was subsequently transferred to a 100 mL autoclave. The hydrogenation reaction began with stirring (1200 rpm) at 363 K after hydrogen (99.999% purity) was introduced into the autoclave. The reaction was stopped after an appropriate time, and then the products were analyzed using a GC-FID (GC-2014, Shimadzu Co.) equipped with a flame ionization detector (FID) and capillary column (DM-WAX, 30 m × 0.25 mm × 0.25 μm). The response factor of each component was calculated using the standard sample and used to calculate the conversion and selectivity.

3. Results and discussion

3.1. Characterization of the catalysts

The Pt/15TS and Pt–FeO_x/15TS catalysts were firstly characterized by low-angle powder XRD. As displayed in Fig. 1, the 15TS composites displayed the typical (100), (110) and (200) diffraction peaks in the region of 2θ = 0.5–2°, which are characteristic of the *P6mm* hexagonal structure of the SBA-15 host. All the Pt-based catalysts possessed the typical mesoporous structure similar to that of the SBA-15 host, demonstrating that the loading of TiO_2 and Pt nanoparticles did not destroy the ordered structure of the SBA-15 host. The mesoporous structure of the Pt-based catalysts was further confirmed by N_2 sorption (Fig. 2) and SEM (Fig. 3). Both the Pt/15TS and Pt–FeO_x/15TS catalysts showed typical type IV isotherms with hysteresis loops, suggesting that they retained the mesoporous structure. For clarity, Table 1 lists the detailed physicochemical parameters of the related samples. On the whole, the pore volume and the BET specific surface area of the Pt/15TS and Pt–FeO_x/15TS catalysts decreased a little compared with those of the SBA-15 host, indicating that the introduced TiO_2 and deposited Pt nanoparticles occupied a certain mesoporous channel. As a result, the Pt/15TS catalyst has a BET specific surface area of 345 m^2 g^{-1}. When FeO_x

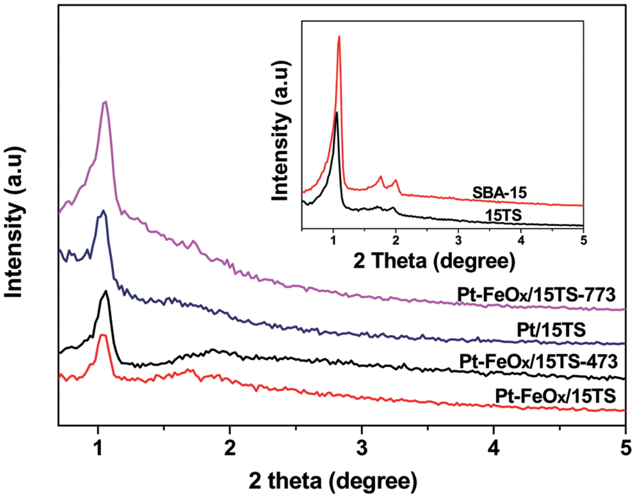

Fig. 1 Low-angle XRD patterns of the Pt/15TS and Pt–FeO_x/15TS-*T* catalysts.

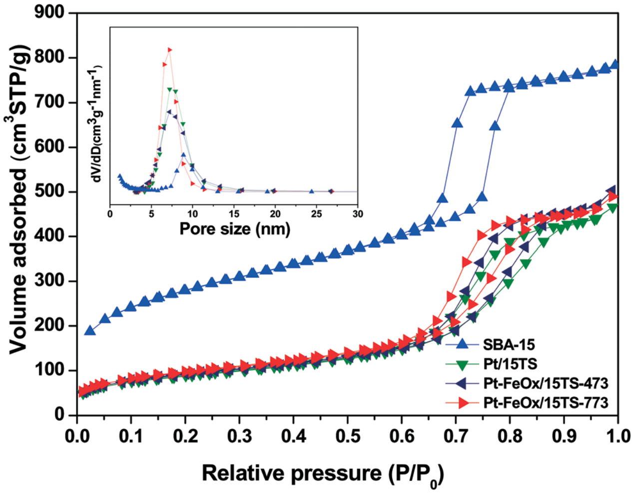

Fig. 2 N_2-physisorption isotherms and pore size distribution of Pt/15TS and Pt–FeO_x/15TS-*T* catalysts.

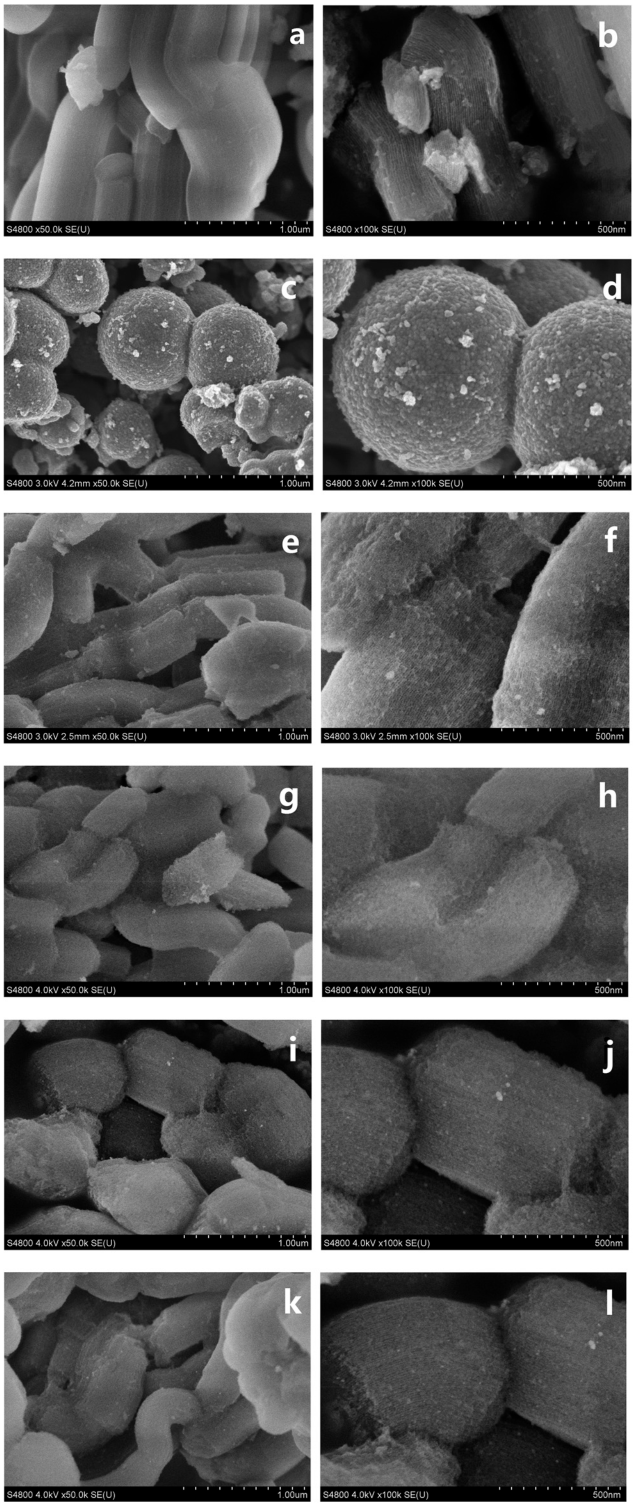

Fig. 3 SEM images of (a and b): SBA-15; (c and d): TiO_2; (e and f): 15TS; (g and h): Pt/15TS; (i and j): Pt–FeO_x/15TS-773; (k and l): used Pt–FeO_x/15TS-773.

was doped to the Pt/15TS catalyst, the BET specific surface area of the Pt–FeO_x/15TS catalyst was in the range of 339 to 349 m^2 g^{-1}. The average pore diameters were in the range of 6.5–7.2 nm as evaluated by the BJH method.

From the SEM images of Fig. 3, sphere-like aggregates larger than 500 nm were detected for pure TiO_2. In contrast, the TiO_2 aggregate size in 15TS composites was much smaller than that of the pure TiO_2, and many well-dispersed TiO_2 aggregates smaller than 30 nm located outside the SBA-15 mesopores were clearly observed. In other words, the growth of TiO_2 particles was greatly restrained when they were coated onto SBA-15. At the same time, addition of Pt or FeO_x did not change its appearance and still maintained the structure of SBA-15.

The wide-angle powder XRD patterns were measured to investigate the crystalline phases of TiO_2 and Pt crystallites. As shown in Fig. 4, there are no distinct TiO_2 crystallite peaks for 15TS composites, further demonstrating that mesoporous SBA-15 can effectively suppress the growth of TiO_2 particles, resulting in high dispersion of TiO_2. Besides, the weak Pt(111) diffraction peak of the Pt/15TS catalyst indicates that the Pt particles are well dispersed on the 15TS composites. Nonetheless, according to the Scherrer equation, the average Pt particle size for the Pt/15TS catalyst centers at 3.2 nm; while for the Pt/SBA-15 and Pt/TiO_2 catalysts, it is focused at 5.8 and 2.0 nm, respectively. The pure TiO_2, with a perfect rutile crystalline phase,[46] can have strong interactions with supported Pt nanoparticles and make them uniformly dispersed on its surface. After coating TiO_2 with 15 wt% loading inside the SBA-15 mesoporous channels, only amorphous titania was formed with a few layers so that the interaction between the amorphous titania and Pt nanoparticles became weaker than that of pure TiO_2 with a perfect rutile crystalline phase. Consequently, the size of Pt particles supported on 15TS composites is bigger than that supported on pure TiO_2. Nevertheless, due to somewhat interaction of Pt nanoparticles with amorphous TiO_2, the average Pt particle size of the Pt/15TS catalyst was smaller than that of the Pt/SBA-15 catalyst.

After FeO_x was doped to the Pt/15TS catalyst, the diffraction peak assigned to Pt crystallites is broader when the

Table 1 Relevant physicochemical parameters of relevant samples

Entry	Catalyst	S_{BET} ($m^2\ g^{-1}$)	V_p ($cm^3\ g^{-1}$)	Pore diameter (nm)
1	SBA-15	830	1.10	8.1
2	Pt/15TS	345	0.73	7.2
3	Pt–FeO_x/15TS-473	349	0.80	6.5
4	Pt–FeO_x/15TS-773	339	0.77	7.2

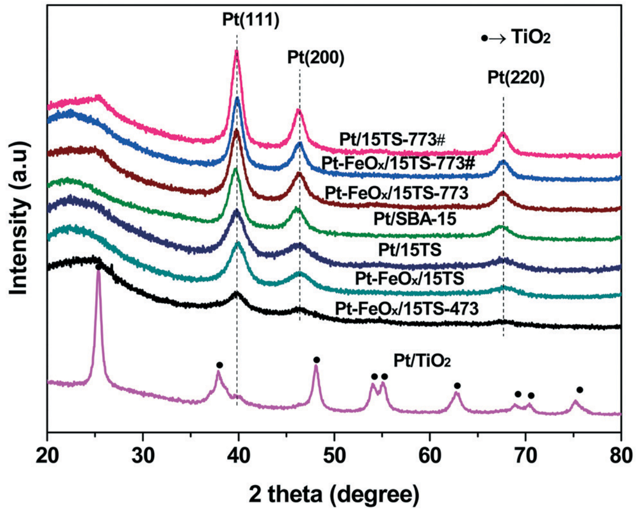

Fig. 4 Wide-angle XRD patterns of the Pt-based catalysts, where # represents the as-calcined sample without reduction.

catalyst precursor was calcined at 473 K before reduction, indicating that Pt nanoparticles with smaller size are dominant on the Pt–FeO_x/15TS-473 catalyst. However, if the catalyst precursor was calcined at a higher temperature like 773 K, the Pt nanoparticles aggregated to form relatively larger particles for the Pt–FeO_x/15TS-773 catalyst. In addition, the weak diffraction peak assignable to TiO_2 at a 2 theta of 25.8° is also detected.[46] The dispersion of Pt particles was also characterized using TEM. As displayed in Fig. 5, the Pt particle size distribution of Pt/15TS is centered at 3.0–4.0 nm, while those for the Pt–FeO_x/15TS-473 and Pt–FeO_x/15TS-773 catalysts are focused at 2.0–3.0 nm and 4.5–5.0 nm, respectively.

3.2. Hydrogenation of CAL with the Pt-based catalysts

The Pt/15TS catalyst was firstly applied to the liquid-phase hydrogenation of CAL. For comparison, the Pt/TiO_2 and Pt/SBA-15 catalysts were also investigated for the tested reaction. As listed in Table 2, the Pt/TiO_2 catalyst gave about 39% CAL conversion and 76% selectivity to COL within 1 h, while the Pt/SBA-15 catalyst showed only 22% CAL conversion and 41% selectivity to COL. When coating TiO_2 with 15 wt% loading onto SBA-15 to form 15TS composites for loading Pt nanoparticles, the Pt/15TS catalyst afforded greatly improved catalytic performance with nearly 90% CAL conversion and a selectivity to COL of 64%. The activity (represented by TOF, defined as the number of moles of converted CAL per mole of Pt active sites per second) could reach 0.41 s^{-1} with the Pt/15TS catalyst, much higher than those obtained with the Pt/TiO_2 and Pt/SBA-15 catalysts, which furnished TOFs of 0.28 s^{-1} and 0.18 s^{-1}, respectively. In addition, the Pt/15TS catalyst afforded slightly lower selectivity to COL by comparison with the Pt/TiO_2 catalyst, but much higher than the Pt/SBA-15 catalyst.

Clearly, the Pt/15TS catalyst showed superior catalytic activity to those catalysts supported on TiO_2 or SBA-15 alone. The enhanced activity of the Pt/15TS catalyst might be caused by the positive effect of the 15TS composites. As for the average Pt particle size for the Pt catalysts supported on different materials, it increases in the order: Pt/TiO_2 < Pt/15TS < Pt/SBA-15, while the activity in terms of TOF values obtained with these Pt catalysts increases in another sequence: Pt/SBA-15 < Pt/TiO_2 < Pt/15TS. Therefore, it is speculated that the Pt particle size is a less influential factor; however, the interaction between the Pt nanoparticles and support would influence the surface electronic properties of Pt nanoparticles and likely cause considerable changes in their activity and selectivity. The 15TS composites contained highly-dispersed TiO_2 with a thin layer coated on the SBA-15 surface and no crystalline phase of rutile or anatase was observed according to the XRD results. The physicochemical properties of highly dispersed and amorphous TiO_2 are quite different from those of bulk TiO_2, so that the interaction with Pt nanoparticles will be somewhat different resulting in different catalytic performances for the supported Pt catalysts toward the selective hydrogenation of CAL to COL.

3.3. Hydrogenation of CAL with the Pt–FeO_x/15TS catalysts

In order to further improve the catalytic performance of the Pt/15TS catalysts, we attempted to modify the Pt/15TS catalysts with FeO_x. Since the optimal Fe/Pt molar ratio was found to be 0.25 in the literature,[24,47] we prepared Pt–FeO_x/15TS catalysts with the Fe/Pt molar ratio of 0.25 and investigated the catalytic performance for the tested reaction. To our delight, both the CAL conversion and COL selectivity were greatly enhanced with the FeO_x-promoted Pt/15TS catalyst. Accordingly, the Pt–FeO_x/15TS catalyst furnished 99.0% CAL conversion and 84.5% selectivity to COL under the same conditions (Table 2) as the Pt/15TS catalyst.

According to the discussion above, compared with the Pt/15TS catalyst, the FeO_x-promoted Pt/15TS catalyst had much higher catalytic ability under the same conditions and CAL was almost fully converted. To explore the superior catalytic performance of the FeO_x-promoted Pt/15TS catalyst to a great extent, the substrate/catalyst molar ratio was increased three times of that for the Pt/15TS catalyst and the dosage of the catalyst was decreased to a half. Table 3 lists the reaction results obtained with the enlarged substrate/catalyst molar ratio. Consequently, the Pt–FeO_x/15TS catalyst showed 41.6% CAL conversion and 82.0% selectivity to COL.

By taking into account that calcination at an elevated temperature may be beneficial for the metal–support interaction,

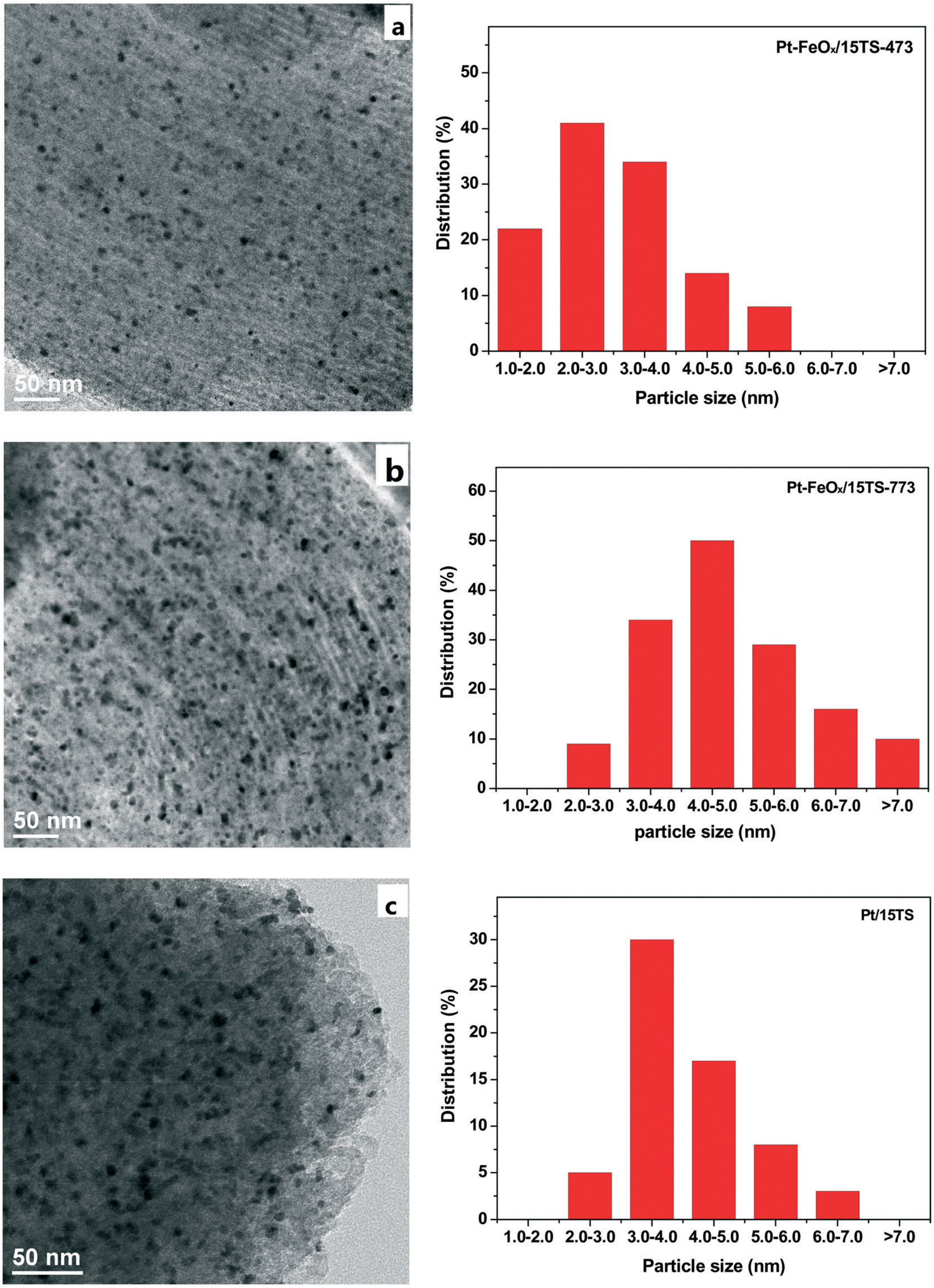

Fig. 5 TEM images and particle size distributions of Pt-based catalysts: (a) Pt–FeO$_x$/15TS-473; (b) Pt–FeO$_x$/15TS-773; and (c) Pt/15TS.

the catalyst precursors were calcined in air at an elevated temperature before reduction in sodium formate solution. To our delight, the Pt–FeO$_x$/15TS-473 catalyst showed a higher conversion of CAL (58.8%), and the selectivity to COL was slightly increased to 83.2%. With the increase of the calcination temperature for the Pt–FeO$_x$/15TS catalyst precursor, the catalytic performance of the Pt–FeO$_x$/15TS-773 catalyst was further improved, which afforded 68.0% CAL conversion and 86.4% selectivity to COL under the same conditions, with the TOF reaching 3.06 s^{-1}, about 7.4 times higher than that with the Pt/15TS catalyst.

Furthermore, to understand the evolution of the hydrogenation product, we also investigated the kinetic behaviors of the selective hydrogenation of CAL with the Pt–FeO$_x$/15TS-

Table 2 Hydrogenation of CAL with different Pt-based catalysts[a]

Entry	Catalyst	Average Pt size[b] (nm)	Disp.[c] (%)	Conv. (%)	TOF[d] (s^{-1})	Sel. (%)		
						COL	HCAL	HCOL
1	Pt/15TS	3.2	35.3	90.0	0.41	64.0	18.4	17.6
2	Pt/TiO_2	2.0	56.5	39.0	0.28	75.7	17.8	6.5
3	Pt/SBA-15	5.8	19.5	22.3	0.18	40.9	46.0	13.1
4	Pt–FeO_x/15TS	3.8	29.7	99.0	1.36	84.5	4.1	11.4

[a] Reaction conditions: 50 mg Pt catalyst; 7.5 mmol CAL; 4.0 MPa H_2; 18 mL isopropyl alcohol + 2 mL water; 1200 rpm; 363 K; 1 h. [b] Pt particle size was calculated from the Scherrer equation. [c] Dispersion was calculated based on dispersion (%) × d (Pt particle size in nm) = 1.13. [d] TOF was defined as the number of moles of converted CAL per mole of Pt active sites per second.

Table 3 Hydrogenation of CAL with different Pt–FeO_x/15TS catalysts[a]

Entry	Catalyst	Average Pt size[b] (nm)	Dispersion[c] (%)	Conv. (%)	TOF[d] (s^{-1})	Sel. (%)		
						COL	HCAL	HCOL
1	Pt–FeO_x/15TS	3.8	29.7	41.6	1.36	82.0	15.5	2.5
2	Pt–FeO_x/15TS-473	2.9	38.9	58.8	1.47	83.2	12.6	4.2
3	Pt–FeO_x/15TS-773	5.2	21.7	68.0	3.06	86.4	9.6	3.9
4	Pt–FeO_x/15TS-773[e]	5.2	21.7	41.2	1.85	68.0	24.0	8.0
5	Pt–FeO_x/15TS-773[f]	—	—	54.6	—	84.3	11.8	3.9

[a] Reaction conditions: 25 mg catalyst; 11.25 mmol CAL; 2.0 MPa H_2; 9 mL isopropyl alcohol + 1 mL water; 0.5 h; 1200 rpm; 363 K. [b] Average Pt particle size (nm) was calculated from the TEM images. [c] Dispersion was calculated based on dispersion (%) × d (Pt particle size in nm) = 1.13. [d] TOF was defined as the number of moles of converted CAL per mole of Pt active sites per second. [e] The reaction was conducted at 303 K. [f] The as-calcined Pt–FeO_x/15TS-773 without reduction or pre-treatment in flowing hydrogen at 673 K was applied.

773 catalyst. As revealed in Fig. 6, the conversion of CAL gradually increased with time and realized complete CAL conversion within 75 min. To our delight, the selectivity to COL of over 86% almost kept unchanged till the full conversion of CAL. If the reaction time was further prolonged, the excessive hydrogenation still proceeded, and as a result, the selectivity to HCOL obviously increased accompanied by the declined selectivity to COL and HCAL.

Moreover, to explore the catalytic activity of the Pt–FeO_x/15TS-773 catalyst to the greatest extent, the CAL hydrogenation was conducted at room temperature as well. As also listed in Table 3, the Pt–FeO_x/15TS-773 catalyst afforded 41.2% CAL conversion with 68.0% selectivity to COL. The selectivity to COL at room temperature was comparatively lower than that obtained at 363 K, because the C=C bond hydrogenation was thermodynamically favored, in accordance with the literature.[48] Nevertheless, the TOF value was still 1.85 s^{-1}, much higher than that with the Pt/15TS catalyst at 363 K.

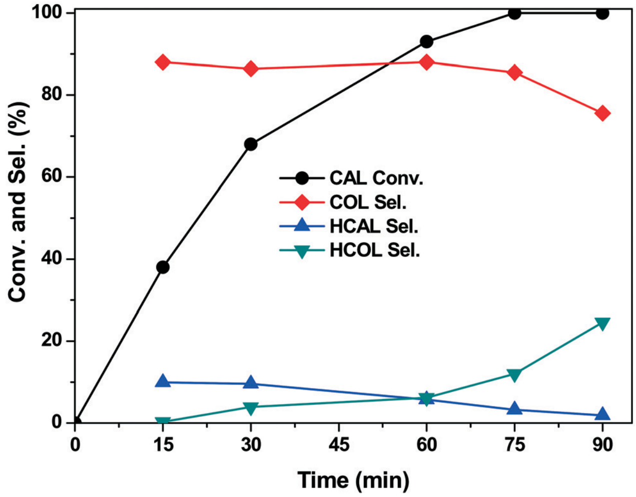

Fig. 6 Kinetic profiles of liquid-phase selective hydrogenation of CAL with the Pt–FeO_x/15TS-773 catalyst. The reaction conditions were identical to those for entry 3 in Table 3 except the reaction time.

Based on the discussion mentioned above, we got to know that the calcination of the catalyst precursor in air at 773 K can greatly enhance the CAL hydrogenation. Compared with the Pt/15TS catalyst, the Pt–FeO_x/15TS catalyst improved the activity and selectivity remarkably, mainly due to the intimate contact of Pt entities with FeO_x.

To fully understand the performance of the Pt–FeO_x/15TS catalyst, the comparison was also made with other Pt–Fe catalysts reported in the literature. For instance, the bimetallic Pt–Fe catalyst supported on mesoporous carbon prepared by the incipient wetness impregnation method afforded a TOF of 0.049 s^{-1}, which was calculated using the results obtained with the 5 wt% Pt–0.8 wt% Fe/C-SA catalyst.[28] The Pt–Fe catalyst supported on the carbon nanotubes prepared by microwave heating gave 0.94–2.21 s^{-1} TOF.[48] These TOF values are lower than that afforded by the Pt–FeO_x/15TS-773 catalyst in the present work. Moreover, for the Pt–FeO_x/SiO_2 catalysts prepared by a galvanic displacement method, the CAL consumption rate normalized to the amount of Pt (MSA_{CAL}, defined as the moles of converted CAL per gram of Pt per hour) was in the range of 0.89–2.24 mol g_{Pt}^{-1} h^{-1},[49] which is much lower than the highest MSA_{CAL} of 12.24 mol g^{-1} h^{-1}

(calculated using the same method as the Pt–FeO_x/SiO_2 catalysts in ref. 49) furnished by the Pt–FeO_x/15TS-773 catalyst in this study. Additionally, the selectivity to COL about 86.4% is also slightly higher than that of the Pt–FeO_x/SiO_2 catalysts (84.0% selectivity at the highest MSA_{CAL}).

In addition, we also made a comparison between the Pt–FeO_x/15TS-773 catalyst in this study and Pt catalysts supported on reduced graphene oxide (RGO) published in the literature. The monometallic Pt/RGO catalyst reached the highest TOF of 26.7 min^{-1} calculated using the total amount of Pt atoms for the selective hydrogenation of CAL with 85.3% selectivity to COL.[23] We noticed that the Pt/RGO catalyst had an average Pt particle size of 2 nm with a dispersion of about 56.5%. According to our calculation method, Pt/RGO afforded a TOF value of 0.79 s^{-1}. Besides, the same group also investigated a Pt_3Sn/SnO_2/RGO hybrid for the selective hydrogenation of unsaturated aldehydes.[29] As a result, the hybrid with 0.6–1.2 nm Pt_3Sn nanoparticles furnished a TOF of 29.1 min^{-1} (0.485 s^{-1}) for the selective hydrogenation of CAL. Although the selectivity to COL (92.5%) with the hybrid catalyst was slightly higher than that with the Pt–FeO_x/15TS-773 catalyst in the present work (86.4%), the Pt–FeO_x/15TS-773 catalyst afforded much higher activity in terms of TOF value (3.06 s^{-1}).

3.4. Reusability of the Pt–FeO_x/15TS catalyst

Reusability is one of the important factors to be considered for heterogeneous catalysts involved in a liquid-phase reaction. Therefore, we investigated the recyclability of the Pt–FeO_x/15TS-773 catalyst toward the liquid-phase hydrogenation of CAL. As a result, the catalyst showed no distinct loss in activity or selectivity to COL even after eight cycles (Fig. 7). Moreover, the CAL conversion presented a volcanic trend. We noticed that higher CAL conversions and COL selectivities were furnished with the used Pt–FeO_x/15TS-773 catalyst after the first run. It can be interpreted that the catalyst surface was reconstructed after the first run and the catalyst surface was more suitable for the selective hydrogenation of CAL to the desired product COL.[47,50] We also detected the Pt leaching amount in the filtrate using ICP-AES and to our delight, the Pt–FeO_x/15TS-773 catalyst is stable and the amount of leached Pt was below the detection limit of ICP-AES, which further demonstrated that Pt nanoparticles were stable enough during the recycling processes. This may be attributed to the strong interaction between Pt–FeO_x and the metal–support, which occurred when the catalyst was calcined and pre-treated in a hydrogen flow at 673 K. The effect would enhance the stability of Pt and effectively prevent leaching of Pt during the recycling processes. Meanwhile, we also characterized the recycled catalyst using SEM. As also displayed in Fig. 3(k and l), the morphology of the used Pt–FeO_x/15TS-773 catalyst still maintained the perfect channel-structure of the SBA-15 host and no TiO_2 particles aggregated on the outer surface. This confirms again that the Pt–FeO_x/15TS-773 catalyst was stable enough so that it can be recovered and reused several times without obvious loss in catalytic performance.

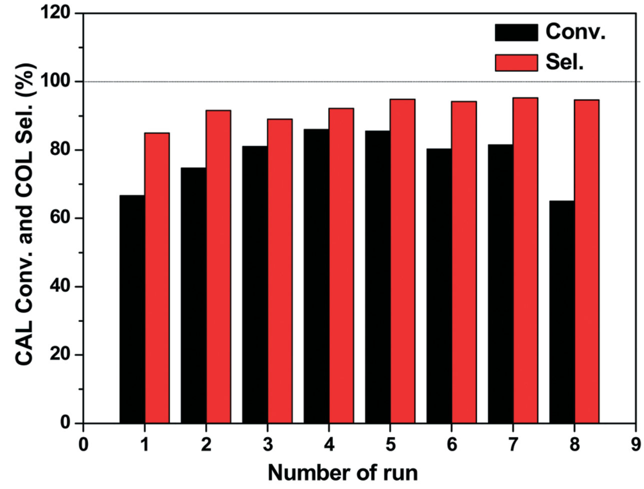

Fig. 7 Reusability of the Pt–FeO_x/15TS-773 catalyst toward the selective hydrogenation of CAL. The reaction conditions are identical to those for entry 3 in Table 3.

With regards to the declined CAL conversion after running eight cycles, there are a few possible reasons. The first one is the gradually decreased catalyst amount. In order to wash out the adsorbed reactant and product on the catalyst surface, the recycled catalyst was washed with isopropyl alcohol and then centrifuged 3–4 times after each cycle. As a result, the total amount of the recycled catalyst decreased due to the inevitable washing away of the catalyst with the solvent, so that the amount of the catalyst subjected to the next run was less than that for the previous cycle. We weighed the catalyst after eight cycles and only 64% of the catalyst was recovered after the eight cycles. The second reason might be that the strongly-adsorbed species occupied the active sites of the Pt–FeO_x/15TS-773 catalyst so that the active sites participating in adsorption and activation of the reactant for the next run are actually decreased. The last possible reason is the slight aggregation of Pt particles during the recycling process.

3.5. Further characterization of the Pt-based catalysts

In order to study the Pt–FeO_x and Pt–support interactions, H_2-TPR was then conducted for the as-calcined Pt–FeO_x/15TS-773 catalyst. For comparison, the similar as-calcined Pt/15TS-773 catalyst without addition of FeO_x was also prepared and studied by H_2-TPR. From Fig. 8, for the as-calcined Pt/15TS-773 sample, there was only one weak but obvious reduction peak centered at around 553 K, which can be attributed to the reduction of PtO_x.[49] As for the as-calcined Pt–FeO_x/15TS-773 catalyst, the reduction of PtO_x was shifted to a higher temperature at 627 K, about 74 K higher than that for the as-calcined Pt/15TS-773 catalyst. This demonstrates that the strong interaction of PtO_x with FeO_x exists in the as-calcined Pt–FeO_x/15TS-773 sample. Besides, a broad H_2-consumption

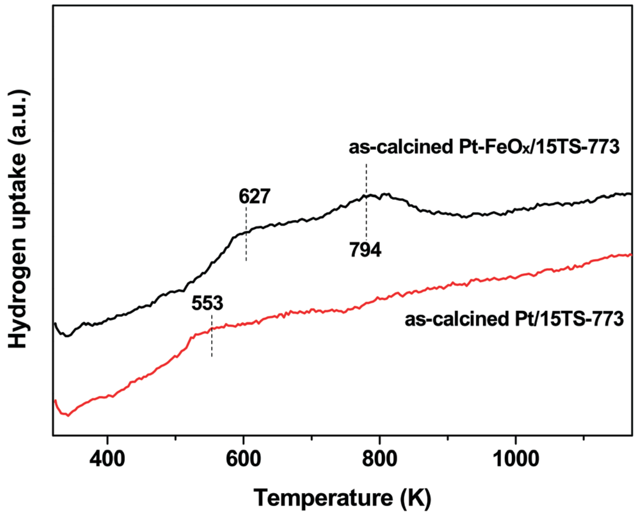

Fig. 8 H_2-TPR profiles for the as-calcined Pt/15TS-773 and the as-calcined Pt–FeO_x/15TS-773 catalysts.

peak due to the reduction of iron oxides at temperatures higher than 794 K was also detected.[49]

Furthermore, we also calculated the H_2 consumption amount of the as-calcined catalyst. Consequently, the H_2 uptake for the as-calcined Pt–FeO_x/15TS-773 catalyst was about 0.009 mmol g^{-1}. The H/Pt ratio was also calculated correspondingly to be about 0.07 for the as-calcined Pt–FeO_x/15TS-773 catalyst, much lower than the stoichiometric value of 4.0 when chloroplatinic acid was completely reduced to Pt^0 species. The possible reason for the extremely low H/Pt ratio is that most Pt precursors in the as-calcined Pt–FeO_x/15TS-773 catalyst already decomposed to Pt^0 species before H_2-TPR measurement, which might occur during calcination in air at 773 K. To verify the Pt crystalline phase for the as-calcined Pt–FeO_x/15TS-773 catalyst, the XRD pattern was measured. As already displayed in Fig. 4, the as-calcined sample showed distinct Pt(111) diffractions, confirming that most of the Pt precursors have decomposed to Pt atoms during calcination in air at 773 K.

Furthermore, we subjected the as-calcined Pt–FeO_x/15TS-773 catalyst to the hydrogenation of CAL. As a result, it gave 54.6% CAL conversion and 84.3% selectivity to COL (Table 3). Although the CAL conversion was lower than that obtained with the Pt–FeO_x/15TS-773 catalyst under the same conditions, the results indicate that the as-calcined Pt–FeO_x/15TS-773 catalyst was already active and selective, verifying that most of the Pt precursors were decomposed to Pt^0 atoms during calcination.

To further characterize the surface electronic properties, the as-calcined Pt–FeO_x/15TS-773 catalyst was probed by XPS. For comparison, the as-calcined Pt/15TS-773 sample was also characterized using XPS as well. As displayed in Fig. 9A, the XPS spectra can be deconvoluted to two Pt species for the as-calcined Pt/15TS-773 and Pt–FeO_x/15TS-773 catalysts, with the Pt $4f_{7/2}$ peaks appearing at 71.0 and 73.0 eV, respectively. According to the literature, the Pt $4f_{7/2}$ peaks observed at 70.7–71.3 eV can be assigned to Pt^0, while the Pt$4f_{7/2}$ peaks at 72.4–74.6 eV could be assigned to PtO.[47,49] Therefore, the

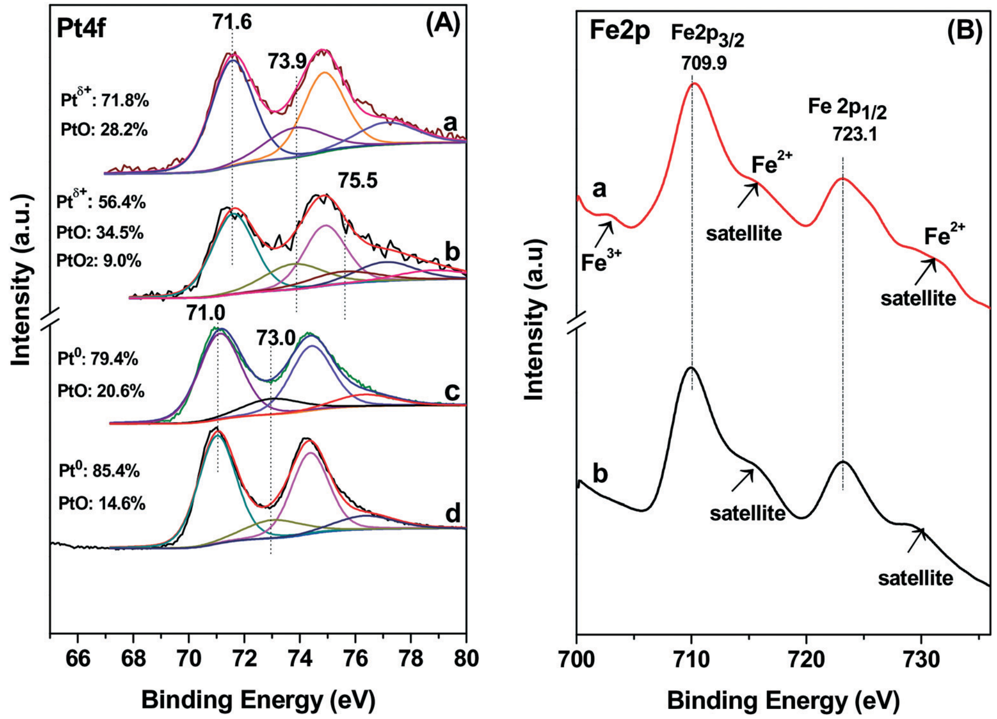

Fig. 9 (A) Pt4f XPS spectra measured after *in situ* pre-treatment in flowing hydrogen at 673 K for 2 h: (a) Pt/15TS-773 and (b) Pt–FeO_x/15TS-773; and Pt4f spectra obtained with the as-calcined samples: (c) Pt–FeO_x/15TS-773 and (d) Pt/15TS-773. (B) Fe2p XPS spectra for the (a) as-calcined Pt–FeO_x/15TS-773 and (b) Pt–FeO_x/15TS-773 catalysts after *in situ* pre-treatment in flowing hydrogen at 673 K for 2 h.

binding energy at 71.0 eV can be assigned to Pt^0 species and that at 73.0 eV was ascribed to Pt^{2+} species. For the as-calcined Pt/15TS-773 catalyst, the relative ratios of Pt^0 and Pt^{2+} are 85.4% and 14.6%, respectively; while for the as-calcined Pt–FeO_x/15TS-773 catalyst, the relative ratios are 79.6% and 20.4%, respectively. The XPS results further confirmed the conclusion of H_2-TPR that most of the Pt precursors in the as-calcined Pt/15TS-773 or Pt–FeO_x/15TS-773 catalysts already decomposed to Pt^0 species. In addition, for the as-calcined Pt–FeO_x/15TS-773 catalyst, there are more Pt^{2+} species on the surface compared with the as-calcined Pt/15TS-773 catalyst, demonstrating that there are strong interactions between Pt species and FeO_x species. Furthermore, the Fe 2p XPS spectrum for the as-calcined Pt–FeO_x/15TS-773 catalyst is also shown in Fig. 9B. The positions of the satellite peaks for the Fe 2p peaks are very sensitive to the oxidation states and these peaks have been used for qualitative determination of the ionic states of iron. For the as-calcined Pt–FeO_x/15TS-773 catalyst, the BE for Fe $2p_{3/2}$ is at about 709.9 eV, with a satellite peak at 715.5 eV, which can be assigned to Fe^{2+}.[51,52] On recalling the experiments in the present work, we introduced $FeCl_3$ with a Fe^{3+} precursor into the catalyst, while the existence of Fe^{2+} species further indicated that more intimate and stronger Pt–FeO_x interactions occurred when the catalyst precursor was calcined in air at 773 K. This is in good agreement with the H_2-TPR results. Due to the strong interaction between Pt–FeO_x, the reduction of the as-calcined Pt–FeO_x/15TS-773 catalyst needs relatively higher temperature when compared with that of the as-calcined Pt/15TS-773 catalyst.

Moreover, in order to understand the promotion effect of FeO_x in the Pt–FeO_x/15TS catalyst on the selective hydrogenation of CAL and to correlate with the reaction results, the XPS measurement of Pt–FeO_x/15TS-773 after *in situ* pre-treatment under a hydrogen flow at 673 K for 2 h was also evaluated by XPS. As also displayed in Fig. 9A, the XPS spectrum can be deconvoluted to three Pt species for the Pt–FeO_x/15TS-773 catalyst, with the Pt $4f_{7/2}$ peaks appearing at 71.7, 74.0 and 75.5 eV, respectively. Since the binding energy at 71.7 eV is higher than that of Pt^0, but lower than that of Pt^{2+}, it can be assigned to $Pt^{\delta+}$ species ($0 < \delta < 2$). The binding energies at 74.0 and 75.5 eV could be ascribed to Pt^{2+} and Pt^{4+} species, respectively. The relative ratios of $Pt^{\delta+}$, Pt^{2+} and Pt^{4+} for the Pt–FeO_x/15TS-773 catalyst are 56.5%, 34.5% and 9%, respectively. For comparison, the Pt/15TS-773 catalyst was also probed by XPS after *in situ* pre-treatment in flowing hydrogen at 673 K for 2 h and the XPS spectrum can be deconvoluted to two species as a result, with the Pt $4f_{7/2}$ peaks appearing at 71.7 and 74.0 eV. Similarly, the Pt/15TS-773 catalyst surface contained 71.8% $Pt^{\delta+}$ and 28.2% Pt^{2+} species.

Compared with the Pt $4f_{7/2}$ peak of the as-calcined Pt/15TS-773 and Pt–FeO_x/15TS-773 catalysts, of which Pt^0 atoms are dominant on the surface with a Pt $4f_{7/2}$ peak at 71.0 eV, there is a 0.7 eV shift to higher BEs for the reduced and pre-treated samples. The shift in the Pt $4f_{7/2}$ peak clearly demonstrated that strong interactions between the 15TS support and Pt particles occurred when the catalysts were pre-treated under a hydrogen flow at 673 K.[53,54] Electron transfer might take place from the Pt nanoparticles to the support.[46,55] In addition, the Pt–FeO_x/15TS-773 catalyst had more Pt^{2+} and Pt^{4+} species on the catalyst surface, revealing that the intimate contact of Pt species with FeO_x and thus the Pt–FeO_x interaction occurred with the electron transfer from Pt to the iron oxides.[47–50,56]

As for the Fe2p XPS spectrum of Pt–FeO_x/15TS-773 after *in situ* pre-treatment in a hydrogen flow at 673 K, it is almost the same as that for the as-calcined Pt–FeO_x/15TS-773 catalyst. This indicates that the Fe species did not change a lot during reduction or pre-treatment under a hydrogen flow at 673 K.

From the discussion mentioned above, there are intimate and strong interactions between Pt and the 15TS support and between Pt and FeO_x. Such interactions changed the electronic properties of Pt nanoparticles and there are predominant electron-deficient $Pt^{\delta+}$ species with more Pt^{2+} and Pt^{4+} species on the surface of the Pt–FeO_x/15TS-773 catalyst. When the Pt–FeO_x/15TS-773 catalyst was used for the hydrogenation, the $Pt^{\delta+}$ species are beneficial for the preferential adsorption and activation of the carbonyl group.[47,50] Moreover, the hydrogenation at the C=O bond was further enhanced by the intimate interactions between Pt–FeO_x entities in which the cationic Fe ions play a role for the selective activation of the C=O bond.[24,47,49] Hence, Pt–FeO_x/15TS-773 exhibited superior performance including the CAL conversion and COL selectivity.

4. Conclusions

TiO_2@SBA-15 composites were prepared *via* a facile sol–gel method and applied for loading Pt nanoparticles towards the liquid-phase hydrogenation of cinnamaldehyde to cinnamyl alcohol. The Pt/TiO_2@SBA-15 catalysts greatly enhanced the selective hydrogenation of CAL compared with Pt catalysts supported on TiO_2 or SBA-15 alone. Furthermore, doping of FeO_x to the Pt/TiO_2@SBA-15 catalyst together with calcination of the catalyst precursor in air at an elevated temperature further improved the catalytic performance. As a result, a TOF value of 3.06 s^{-1} was furnished by the Pt–FeO_x/TiO_2@SBA-15-773 catalyst, about 7.4 times higher than that with the Pt/TiO_2@SBA-15 catalyst. It is noteworthy that 86.4% selectivity to COL can be furnished over the Pt–FeO_x/TiO_2@SBA-15-773 catalyst. The most remarkable feature of the Pt–FeO_x/TiO_2@SBA-15-773 catalyst is that it could be recycled at least eight times without distinct loss in activity or selectivity to COL. By combination of the spectroscopic and temperature-programmed characterization techniques, it was proved that there are strong interactions between Pt and TiO_2@SBA-15 composites and also between Pt–FeO_x, resulting in that the electron-deficient $Pt^{\delta+}$ species are dominant on the catalyst surface. The electron-deficient $Pt^{\delta+}$ species, together with Fe^{2+} species, in the Pt–FeO_x/TiO_2@SBA-15-773 catalyst are helpful for the preferential adsorption and activation of the carbonyl group, thus furnishing greatly improved catalytic performance towards the selective hydrogenation of CAL to COL.

Conflicts of interest

There are no conflicts of interest to declare.

Acknowledgements

This work was supported by the National Natural Science Foundation of China (21273076 and 21373089), the Open Research Fund of Top Key Discipline of Chemistry in Zhejiang Provincial Colleges and Key Laboratory of the Ministry of Education for Catalysis Materials (Zhejiang Normal University) (ZJHX2013), and the Shanghai Leading Academic Discipline Project (B409).

References

1 J. P. Stassi, P. D. Zgolicz, S. R. de Miguel and O. A. Scelza, *J. Catal.*, 2013, **306**, 11–29.

2 J. Teddy, A. Falqui, A. Corrias, D. Carta, P. Lecante, I. Gerber and P. Serp, *J. Catal.*, 2011, **278**, 59–70.

3 Y. Yuan, S. Yao, M. Wang, S. Lou and N. Yan, *Curr. Org. Chem.*, 2013, **17**, 400–413.

4 S. Bhogeswararao and D. Srinivas, *J. Catal.*, 2012, **285**, 31–40.

5 B. H. Zhao, J. G. Chen, X. Liu, Z. W. Liu, Z. Hao, J. Xiao and Z. T. Liu, *Ind. Eng. Chem. Res.*, 2012, **51**, 11112–11121.

6 X. Chen, H. Li, W. Dai, J. Wang, Y. Ran and M. Qiao, *Appl. Catal., A*, 2003, **253**, 359–369.

7 Z. Tian, Q. Li, Y. Li and S. Ai, *Catal. Commun.*, 2015, **61**, 97–101.

8 D. Loffreda, F. Delbecq, F. Vigné and P. Sautet, *J. Am. Chem. Soc.*, 2006, **128**, 1316–1323.

9 C. Vriamont, T. Haynes, E. Mccague-Murphy, F. Pennetreau and S. Hermans, *J. Catal.*, 2015, **329**, 389–400.

10 X. Yang, D. Chen, S. Liao, H. Song, Y. Li, Z. Fu and Y. Su, *J. Catal.*, 2012, **291**, 36–43.

11 K. Q. Sun, Y. C. Hong, G. R. Zhang and B. Q. Xu, *ACS Catal.*, 2014, **1**, 1336–1346.

12 A. K. Prashar, S. Mayadevi and R. Nandini Devi, *Catal. Commun.*, 2012, **28**, 42–46.

13 K. R. Kahsar, D. K. Schwartz and J. W. Medlin, *J. Am. Chem. Soc.*, 2014, **136**, 520–526.

14 S. Handjani, E. Marceau, J. Blanchard, J. M. Krafft and M. Che, *J. Catal.*, 2011, **282**, 228–236.

15 W. Lin, H. Cheng, L. He, Y. Yu and F. Zhao, *J. Catal.*, 2013, **303**, 110–116.

16 Q. Yu, X. Zhang, B. Li, J. Lu, G. Hu, A. Jia, C. Luo, Q. Hong, Y. Song and M. Luo, *J. Mol. Catal. A: Chem.*, 2014, **392**, 89–96.

17 M. Chatterjee, Y. Ikushima and F. Zhao, *New J. Chem.*, 2003, **27**, 510–513.

18 C. Li, Z. Shao, M. Pang, C. T. Williams, X. Zhang and C. Liang, *Ind. Eng. Chem. Res.*, 2012, **51**, 4934–4941.

19 E. Castillejos, M. Jahjah, I. Favier, A. Orejón, C. Pradel, E. Teuma, A. M. Madseu Bulto, P. Serp and M. Gomez, *ChemCatChem*, 2012, **4**, 118–122.

20 P. D. Zgolicz, J. P. Stassi, M. J. Yanez, O. A. Scelza and S. R. de Miguel, *J. Catal.*, 2012, **290**, 37–54.

21 M. Niu, Y. Wang, L. I. Wenjiang, J. Jiang and Z. Jin, *Chin. J. Catal.*, 2013, **34**, 674–678.

22 K. R. Kahsar, S. Johnson, D. K. Schwartz and J. W. Medlin, *Top. Catal.*, 2014, **57**, 1505–1511.

23 J. Shi, R. Nie, P. Chen and Z. Hou, *Catal. Commun.*, 2013, **41**, 101–105.

24 P. Gallezot and D. Richard, *Catal. Rev.: Sci. Eng.*, 1998, **40**, 81–126.

25 A. Siani, O. S. Alexeev, G. Lafaye and M. D. Amiridis, *J. Catal.*, 2009, **266**, 26–38.

26 Y. Li, P. F. Zhu and R. X. Zhou, *Appl. Surf. Sci.*, 2008, **254**, 2609–2614.

27 Z. Guo, Y. Chen, L. Li, X. Wang, G. L. Haller and Y. Yang, *J. Catal.*, 2010, **314**, 276–326.

28 N. Mahata, F. Gonçalves, M. F. R. Pereira and J. L. Figueiredo, *Appl. Catal., A*, 2008, **339**, 159–168.

29 J. Shi, M. Zhang, W. Du, W. Ning and Z. Hou, *Catal. Sci. Technol.*, 2015, **5**, 3108–3122.

30 P. Kluson and L. Cerveny, *Appl. Catal., A*, 1995, **128**, 13–31.

31 S. J. Tauster and S. C. Fung, *J. Catal.*, 1978, **55**, 29–35.

32 T. Ekou, L. Ekou, A. Vicente, G. Lafaye and S. Pronier, *J. Mol. Catal. A: Chem.*, 2011, **337**, 82–88.

33 P. Claus, S. Schimpf, R. Schodel, P. Kraak, W. Morke and D. Honicke, *Appl. Catal., A*, 1997, **165**, 429–441.

34 M. Bidaoui, C. Especel, N. Bouchenafa-Saib, D. Duprez and O. Mohammedi, *Appl. Catal., A*, 2012, **445**, 14–25.

35 M. Abid, V. Paul-Boncour and R. Touroude, *Appl. Catal., A*, 2006, **297**, 48–59.

36 A. Dandekar and M. A. Vannice, *J. Catal.*, 1999, **183**, 344–354.

37 S. A. D. S. Corradini, G. G. Lenzi, M. K. Lenzi, C. M. F. Soares and O. A. A. Santos, *J. Non-Cryst. Solids*, 2008, **354**, 4865–4870.

38 J. S. Ratliff, S. A. Tenney, X. Hu, S. F. Conner, S. Ma and D. A. Chen, *Langmuir*, 2009, **25**, 216–225.

39 T. Ekou, C. Especel and S. Royer, *Catal. Today*, 2011, **173**, 44–52.

40 P. Cheng, M. Zheng, Y. Jin, Q. Huang and M. Gu, *Mater. Lett.*, 2003, **57**, 2989–2994.

41 H. Chun, Y. Wang and H. Tang, *Appl. Catal., B*, 2001, **30**, 277–285.

42 L. A. Cano, M. V. Cagnoli, N. A. Fellenz, J. F. Bengoa, N. G. Gallegos, A. M. Alvarez and S. G. Marchetti, *Appl. Catal., A*, 2010, **379**, 105–110.

43 Y. Tang, S. Miao, B. H. Shanks and X. Zheng, *Appl. Catal., A*, 2010, **375**, 310–317.

44 X. Li, W. Zheng, H. Pan, Y. Yu, L. Chen and P. Wu, *J. Catal.*, 2013, **300**, 9–19.

45 D. Zhao, J. Feng, Q. Huo, N. Melosh, G. H. Fredrickson, B. F. Chmelka and G. D. Stucky, *Science*, 1998, **279**, 548–552.

46 Q. Wu, C. Zhang, B. Zhang, X. Li, Z. Ying and F. Zhao, *J. Colloid Interface Sci.*, 2016, **463**, 75–82.

47 H. Pan, J. Li, J. Lu, G. Wang, W. Xie, P. Wu and X. Li, *J. Catal.*, 2017, **354**, 24–36.

48 Z. Guo, C. Zhou, D. Shi, Y. Wang, X. Jia and J. Chang, *Appl. Catal., A*, 2012, **435**, 131–140.

49 Y. S. Shi, Z. F. Yuan, Q. Wei, K. Q. Sun and B. Q. Xu, *Catal. Sci. Technol.*, 2016, **6**, 7033–7037.

50 R. Yao, J. Li, P. Wu and X. Li, *RSC Adv.*, 2016, **6**, 81211–81218.

51 P. C. J. Graat and M. A. J. Somers, *Appl. Surf. Sci.*, 1996, **100**, 36–40.

52 T. Yamashita and P. Hayes, *Appl. Surf. Sci.*, 2008, **254**, 2441–2449.

53 A. Lewera, L. Timperman, A. Roguska and N. Alonso-Vante, *J. Phys. Chem. C*, 2011, **115**, 20153–20159.

54 X. Y. Liu, A. Wang, T. Zhang and C. Y. Mou, *Nano Today*, 2013, **8**, 403–416.

55 M. S. Kim, S. H. Chung, C. J. Yoo, M. S. Lee, I. H. Cho, D. W. Lee and K. Y. Lee, *Appl. Catal., B*, 2013, **142**, 354–361.

56 M. Li, X. Chen, J. Guan, X. Wang, J. Wang, C. T. Williams and C. Liang, *J. Mater. Chem.*, 2011, **22**, 609–616.